

Fitting analytical BRDF models to low-resolution measurements of light scattered from relief printing samples

Ni Yan^a; Teun Baar^b; Maria Ortiz Segovia^b; Jan Allebach^a; ^aSchool of Electrical and Computer Engineering, Purdue University, West Lafayette, IN 47906, U.S.A.; ^bOcé – Canon Group, France

Abstract

2.5D/3D printing brings new perspectives in many fields, such as manufacturing, architecture, and arts. These new applications also bring out the issues that were barely considered in traditional 2D printing and go beyond color accuracy. Given the recent possibilities of surface construction, one may wonder how the texture details affect the reflection properties of a relief print. In this paper, we attempt to address this question by designing and testing on two groups of relief printed samples: 25 textured surfaces with different roughness levels and 40 visually flat surfaces with different gloss levels. We will first describe how reflection data (in the form of BRDFs) was acquired with our test device. Then we fit the data with some current analytical BRDF models. The results show that, in terms of accuracy and speed, the Ward model fitting outperforms the other models we use. On the other hand, we see that for our rough surface samples, there is a weak positive correlation between input roughness and the roughness parameter in microfacet based Cook-Torrance model. This parameter, however, shows a stronger negative correlation to surface gloss level for the flat samples. These results provide a useful insight to the reflection and texture properties of relief prints, and can be further embedded in the printing pipeline.

1. Introduction

2.5D/3D printing was invented in 1980s and has gained more attention recently. It has a variety applications in architecture, medical, fashion, arts, and etc. Due to different needs of the industry, 2.5D/3D printing technology are developed towards different directions. Compared against other available 2.5D/3D products, Océ 2.5D or relief printing stands out by creating prints with protruding surfaces that exhibit a large color gamut and high spatial resolution [1]. Considering this particularity of our relief printer, we want to investigate the accuracy of printed surfaces, and therefore, the degree of surface appearance variations we were able to achieve with our prints. With the additional dimension, 2.5D/3D printing presents more complicated issues regarding lighting and shadowing than typical 2D printing. Thus, traditional 2D image quality evaluation methods are not enough to satisfy the needs of the new printable dimension. However, there are existing methods in the area of optics that may help us understand these new challenges in printing. This is what brings our attention to BRDFs (Bidirectional Reflection Distribution Functions), which are mathematical functions describing the ratio of reflected light over incident light. These functions have been widely used in the area of computer graphics to render lightness of surfaces of 3D objects on a display. These lighting effects are one of the key aspects to produce a realistic look. There are some pioneering works studying how to use a given BRDF input to back engineer its surface distribution to afterwards fabricate a custom surface reflectance [2][3][4]. In order to fully exploit these studies, we need to continue investigating our printer's capabilities and ink properties.

With the intention of obtaining new tools to analyze and control surface properties of relief prints, we measure BRDF data of both flat and textured relief printed surfaces and fit the data to typical analytical BRDF models. These prints are produced with a wet-on-dry relief printer, i.e. one layer of wet ink is printed and cured with UV light, then another layer is printed on top of it. The 40 flat samples are printed at 100% coverage with one of 5 basic ink colors, namely cyan, magenta, yellow, black, and white. Each sample is printed with different printing setups, which result in 8 different gloss levels. The 25 textured samples are also printed at 100% coverage with each basic ink color. They exhibit 5 different isotropic roughness levels. The texture and roughness are realized by varying the height of each pixel using a Gaussian random field. The BRDF data is acquired with a commercially available BRDF test device*. This device only allows four incident light directions, and produces scattering measurements with resolution of 1° for each of these incident angles. We fitted four different analytical BRDF models to the acquired data: two empirical models — the Blinn-Phong model [5] and the Ward model [6], and two microfacet-based models — the Cook-Torrance model [7] and the Ashikhim-Shirley model [8]. The fitting results yield some useful information about the relief printed surfaces.

In Sec. 2.1, we first briefly describe the spherical coordinate system that we use to characterize the BRDF. Then we explain how to relate the image output of the test device to the BRDF. Section 2.2 introduces the analytical models and fitting error matrix we use. In Sec. 3.1, we compare the fitting performance of these analytical models with our relief prints. Lastly, Secs 3.2 and 3.3, respectively, compare surface roughness — a parameter of the input height map, and surface gloss level — measured with a gloss meter, to the Cook-Torrance model fitting results.

2. BRDF data acquisition and analytical model fitting

2.1 BRDF data acquisition

The BRDF is a mathematical model to characterize the relationship between reflected energy and incident energy when light hits a surface. It is usually defined as

$$F = \frac{dL_v}{dE_l}, \quad (1)$$

where L_v is radiance (i.e. reflected light) at viewing direction v , E_l is irradiance (i.e. incident light) at incident light direction l , and dL_v and dE_l represent the energy in a unit of solid angle. As shown in Fig. 1, the vectors of the incident light direction and reflected light direction are expressed in spherical coordinates, where vectors can be specified by two parameters: the azimuth angle ϕ ($0-2\pi$) and the polar angle θ ($0-\pi/2$). The former is defined as the angle of the orthogonal projection of the vector onto a reference plane that passes through the origin and is orthogonal to the zenith, measured from a fixed reference direction in that plane.

And the latter is defined as the angle between the surface normal or zenith and the vector.

*Mini-Diff, Light Tec - Pôle d'Activités Hyérois, 1128 route de Toulon, 83400 Hyères, France

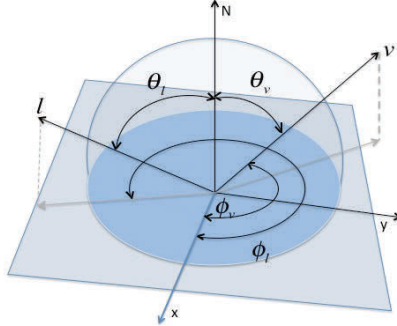


Figure 1. Spherical coordinates, including azimuthal angle ϕ and polar angle θ . N is the normal vector of the surface, $v = (\theta_v, \phi_v)$ is the viewing direction vector, and $l = (\theta_l, \phi_l)$ is the incident light direction vector.

In this paper, as mentioned previously, we use a commercially available image-based test device to obtain BRDF data. It has four incident light angles in a single plane that is perpendicular to the test sample surface. The vectors describing the incident light present the same ϕ_l while their θ_l s are different, namely 0° , 20° , 40° , 60° . For each incident angle, the measurement device detects reflectance with a range for θ_v that goes from 0° to 75° , and ϕ_v from 0 to 2π . The detection resolution is 1° for both θ_v and ϕ_v . The light source is red with a wavelength of 630 nm with spot radius size of 2 mm.

The output data is in the form of four 181×181 2D matrices/images. Each matrix/image is a heat map of reflection strength for each incident angle. Let the top left pixel's coordinate be $(0, 0)$ and the center pixel $(x_0, y_0) = (90, 90)$. With the center pixel being the pole, each pixel (x, y) in the image has equivalent polar coordinates (r, θ) , where $r^2 = (x - x_0)^2 + (y - y_0)^2$, $\theta = \tan^{-1} \frac{y - y_0}{x - x_0}$. θ is equivalent to the azimuth angle ϕ_v in the 3D spherical coordinates, and the radius coordinate r is proportional to the polar angle θ_v in spherical coordinates: $\theta_v = \frac{r}{90} \cdot \frac{\pi}{2}$. Equations (2) to (4) show how to convert the data from 3D spherical coordinates to the 3D Cartesian ones, where the value f of each pixel (x, y) is the BRDF data at the viewing angle (θ_v, ϕ_v) .

$$x = f \cdot \sin \theta_v \cdot \cos \phi_v, \quad (2)$$

$$y = f \cdot \sin \theta_v \cdot \sin \phi_v, \quad (3)$$

$$z = f \cdot \cos \theta_v. \quad (4)$$

Figure 2 is an example of the visualization of the BRDF data we acquired for a print samples.

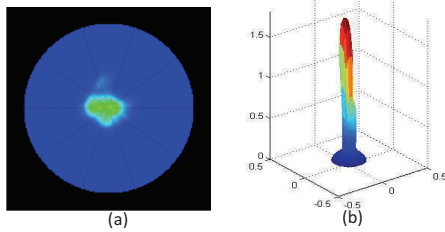


Figure 2. BRDF data 3D visualization. (a) and (c) are the test device output images for the same material, acquired with incident angles 0° and 60° respectively. Within the blue circle is the detective range. (b) and (d) are the 3D Cartesian coordinate visualizations of (a) and (c).

2.2 Analytical model fitting

Acquiring full BRDF data for every viewing and lighting angle of a material requires complex experimental setups and consumes a lot of time [9]. Analytical BRDF models, such as the Lambertian and Phong models, are mathematical approximations with intuitive and adjustable parameters [10]. Fitting real measurements with analytical models is an important procedure to simplify calculations, and reduce storage for the data. Furthermore, analytical models can be used to approximate the BRDF data where a desired pair of incident and viewing angle is not available from the measurements. It also helps to understand the properties of a surface; as the parameters of the fitted model can be used for intuitive interpretation and analysis.

The interaction of light with any surface is a complicated energy transfer process involving reflection, refraction, emission, energy absorption, among other phenomena. However, we can generally characterize two types of surface reflection: specular reflection, the reflection around mirror direction; and diffuse reflection, the reflection that goes evenly across all directions on top of the surface. As we can see in Fig. 2, a real surface can have both of these two reflections. Analytical models simulate lobe shapes to characterize reflections. With a combination of two or even more of them, we can simulate real life surface reflectance. Common models may exhibit different behaviors with different types of surfaces. Some models are more suitable to model smooth surfaces, and some are more suitable to characterize rough surfaces. A single model can hardly consider all the aspects precisely. The more aspects it encompasses, the more complicated it can be. However, among the current models, we can find some parameters in common, like the following:

m : controls the width of the specular lobe

ρ_s : controls the strength of specular lobe

ρ_d : controls the strength of diffuse lobe

F_0 : Fresnel coefficient, reflectance when the light hits a material surface in the direction of the normal vector.

For instance, the specular component F_s of the Ward BRDF model [6] is:

$$F_s(l, v) = \frac{\rho_s}{\sqrt{(N \cdot l)(N \cdot v)}} \cdot \frac{\exp[-\tan^2 \theta_h / m^2]}{4\pi m^2}, \quad (5)$$

where $l = (\theta_l, \phi_l)$ is the lighting direction vector, $v = (\theta_v, \phi_v)$ is the viewing direction vector, h is half vector defined by $h = (l + v) / 2|l + v|$, N is the normal vector of the surface, and ρ_s is the specular reflectance coefficient.

The Lambertian model is commonly used for the diffuse component F_d , for which the result is a constant for every pair of incident and viewing angles:

$$F_d(l, v) = \frac{\rho_d}{\pi}, \quad (6)$$

where ρ_d is the diffuse reflectance coefficient.

In general, a simulated BRDF will have the form:

$$F_m = F_s + F_d, \quad (7)$$

In our case, we adopted the error matrix in [9] and modified it to get the MSE (mean square error) as following:

$$E = \frac{\sum_i \sum_v w_v [F_r(l_i, v) \cdot \cos \theta_{l_i} - F_m(l_i, v) \cdot \cos \theta_{l_i}]^2}{\sum_i \sum_v w_v}, \quad (8)$$

In Eq. (8), $F_r(l_i, v)$ is the measurement data at incident angle l_i and viewing angle v , and $F_m(l_i, v)$ is the simulated data for the same (l_i, v) . The sum is calculated over values of $F_r(l_i, v)$ where measurements have been acquired. The weight w_v is the solid angle correction term. As our data is scattered with 1° resolution, and the distance between the surface and the sensor is much bigger than the diameter of the solid angle projection onto the detection sphere, the angle correction is not significant in our calculations. Thus we set $w_v = 1$. We do not include values of θ_v larger than 75° as measurements with $\theta_v > 75^\circ$ were not available due to the nature of our device. The analytical model parameters of Eq. (7) are found by minimizing E using unconstrained nonlinear optimization. Figure 3 contains an example of a fitting result using the Cook-Torrance model. Each 3D plot shows the measured data in red and the fitted model in blue. Another visualization of the same fitting result is shown in Fig. 4, where a slice of the 3D graph in the incident plane is presented. Measured and simulated data of all four incident angles are plotted together.

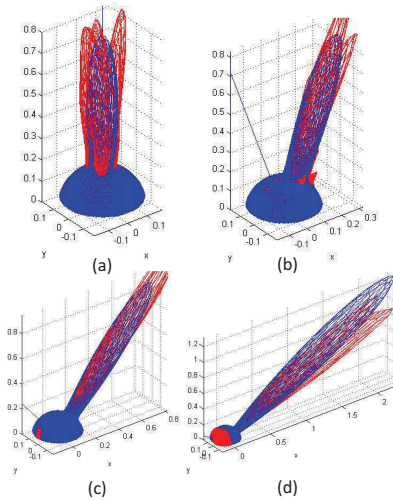


Figure 3. Fitting the BRDF measurement of a print sample with the Cook-Torrance model. From (a) to (d) are the measurement (red mesh) and simulated (blue mesh) data with incident angles 0° , 20° , 40° , 60° , respectively.

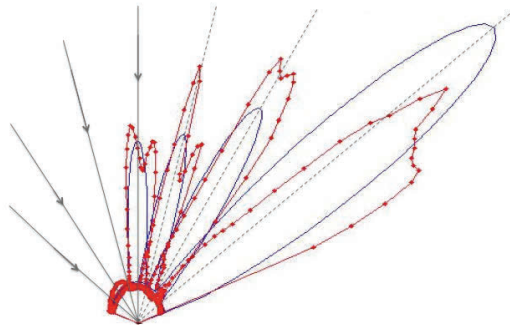


Figure 4. Slice view of the fitting results shown in Fig. 3. Red dots are the measured data, blue is the simulated model fitted to the measurements.

Arrow lines shows incident directions, dashed lines show the corresponding mirror direction.

3. Test of relief printing

We designed and printed two groups of samples, one consisting of visually flat relief prints with different colors and gloss levels and another set composed of textured relief prints with different colors and surface roughness levels. We first test the fitting performance of four analytical BRDF models with our flat samples.

3.1 Fitting performance of analytical BRDF models

The first test is conducted with all the print samples of these two groups. How are these samples are designed and printed will be discussed in the following sections. We obtained the scattering measurements for each of the samples with our device and fitted 4 analytical BRDF models to the data: Blinn-Phong, Cook-Torrance, Ashikhmin-Shirley, and Ward. The average BRDF value (*Ave*), as in Eq. (9), is calculated across all the print samples with each incident angle. We normalized the MSE (as in Eq. (8)) with the *Ave*, and plot the result in Fig. 5. The samples are sorted in an order so that Cook-Torrance fitting error increases from sample 1 to sample 40.

$$Ave = \frac{\sum_i \sum_v F_r(l_i, v)}{\sum_i \sum_v 1}, \quad (9)$$

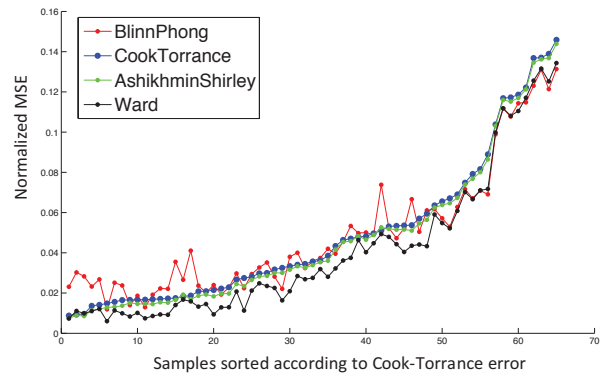


Figure 5. Normalized MSE obtained with tested models when applied to all print samples.

As shown in the plot, the Ward model generally has the best performance throughout our samples. The Blinn-Phong model, which is also an empirical model, has similar behavior to the Ward but exhibits larger errors. Ashikhmin-Shirley and Cook-Torrance are both microfacet-based models, and as we can see from the plot, there is also a consistent similar behavior between them. According to previous studies [12], Ward performs well with varnished wood surfaces, Ashikhmin-Shirley with polished surfaces, Cook-Torrance with metal and plastic, and Blinn-Phong with rough surfaces. The results we have correspond well to previous observations with the Ward model, as the ink we use is fairly glossy. In addition to the outperformance in sense of accuracy, the Ward model is physics-based, and requires less computation than the other models. These fitting results provide useful data for further applications such as realistic 3D simulation for our relief prints. In particular, the Ward model could enable relief printing designers to quickly render 3D files to yield a more realistic preview of their designs before printing.

3.2 BRDF versus surface roughness

Despite the good performance of Ward model, we continue to be interested in microfacet models due to their intuitive representation of surface physical structure.

The modelling of BRDF is difficult due to two aspects. First, the characterization of a surface geometry. In general, there are two popular categories to model a real surface mathematically: random process and V-cavity [15][16]. Previous studies have used V-cavity in BRDF reproduction. Compared with the V-cavity model, the random process method does not require a strong geometrical realization for our printer. For the purpose of understanding prints roughness with BRDF relationship, we generate textured rough surfaces using the Gaussian random process as proposed in [14]. With our printer resolution, we are able to produce very small surface units, each consisting of a single drop of ink. By adding units in a dispersed manner on the printed surface, we can modify its visible roughness texture. As our samples are printed with full ink coverage, these drops connect to the neighbors and form slopes. Figure 6 demonstrates a generated rough surface height map that obeys the Gaussian distribution rule. It is true that due to irregularities and unknown variables in the printing process, the roughness of the prints is not exactly as it is in the input map. However, the actual roughness is strongly correlated with the input random field variance making it an adequate method to generate a surface model. Next, we examine whether or not our BRDF data supports this observation.

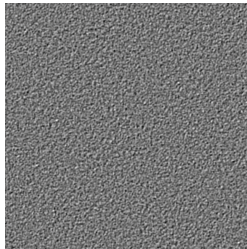


Figure 6. Example of textured surface height map generated with Gaussian random field. The pixel value is proportional to the height (black = 0, white = 0.3 mm).

The second aspect of difficulty of the problem is the light interaction with a surface geometry. As shown in Fig. 3.7, when lights hit a surface, direct reflection, refraction, and absorption can happen. And the reflected rays can bounce multiply times before they can get out of the surface geometry, thus be possible for observers to see.

The Cook-Torrance model simplifies both aspects by, first, assuming that a surface is composed of perfectly reflective (mirror like) microfacets [13]. Thus, for a given incident and viewing direction (l, v) , only facets that have the norm of $h = (l + v)/2|l + v|$ can reflect light into the direction v . The reflection can be, therefore, characterized by the distribution of normal vectors of the facets. The model can be expressed as follows:

$$F_m(l, v) = F_m(\theta_l, \varphi_l; \theta_v, \varphi_v) = \frac{k_d}{\pi} + \frac{k_s}{\pi} \frac{F \cdot D \cdot G}{\cos \theta_l \cos \theta_v}. \quad (10)$$

Here, k_d and k_s are the diffuse and specular coefficients, respectively. F is the Fresnel factor, which can be approximated as in Eq. (11). G , as in Eq. (12), is the geometrical attenuation factor that takes shadowing effects in to account. n is the normal of a microfacet, and the “ \cdot ” symbol implies dot product. In the end, D is the microfacet distribution function shown in Eq. (13), which follows a Gaussian distribution.

$$F = F_0 + (1 - F_0)(1 - (l \cdot h))^5, \quad (11)$$

$$G = \min \left(1, \frac{2(n \cdot h)(n \cdot v)}{(v \cdot h)}, \frac{2(n \cdot h)(n \cdot l)}{(v \cdot h)} \right), \quad (12)$$

$$D = \frac{1}{m^2 \cos^4 \theta_h} e^{-\left(\frac{\tan \theta_h}{m}\right)^2}. \quad (12)$$

The root mean square (rms) parameter m in D controls the variance of the distribution, thus it is positively correlated to the surface roughness. The smaller m is, the more concentrated the distribution of the surface is around the specular reflection direction. On the contrary, large m implies facets normal distribution are more spread out, thus the light reflected from such a surface is more diffused.

We printed 5 roughness levels of such random field for each of our printer’s primary color (namely, CMYKW), resulting in 25 test samples in total. These samples are printed with 100% ink coverage. The maximum pixel height is set to be 0.3mm, and the lowest possible height is 0. We measured the BRDF of these samples and fitted the Cook-Torrance model to the data. The m parameters from the fitting result are shown in Fig. 7, where the x-axis is the standard deviation of the Gaussian random process. As we can see from the plot, whenever the standard deviation goes from 1 to 5, the parameter m generally increases. It indicates that the lobe of the specular reflection grows wider, or equivalently, the reflecting light is more diffused. The increase of Gaussian random field variances causes the increase surface roughness levels. This increase is the causes of surface diffusion, which fits our expectations.

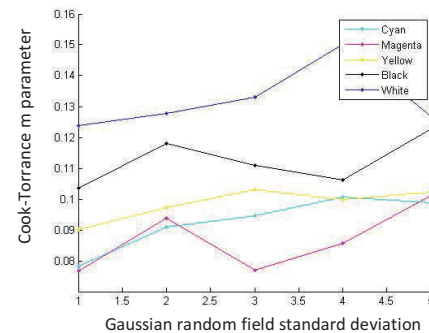


Figure 7. Comparing textured printed samples input Gaussian random process standard deviation with Cook-Torrance roughness parameter.

3.3 BRDF versus gloss measurements

From the obtained scattering measurements (examples in Figs. 2 and 3), it can be seen that the BRDF functions of the printed patches show similar characteristics among them, differing majorly in the width and strength of the specular lobe. We expect that these differences can be well distinguishable with a more simple measurement system such as a gloss meter. To investigate this hypothesis, the BRDF measurements of the set of visually flat patches were compared to the measurements of the glossiness. These samples consist of 40 print samples, also with 100% coverage of one of the 5 primary ink colors, and each color variation printed with 8 different levels of gloss. The different levels of gloss were achieved by using a gloss management workflow, where the gloss level of each print is influenced by the micro scale surface roughness corresponding to different print parameters [11]. These print parameters range from the use of single-pass and multi-pass print modes or the addition of varnish,

to printer settings affecting the deposition and drying processes of the ink such as UV light intensity and droplet size, among other printer settings. For the gloss measurements, a MG628-F2 multi-angle gloss meter was used, where the gloss value is measured in gloss units (GU), with a GU defined such that a glossy material with a refractive index of 1.567 has the value of 100 GU for any illumination angle, according to the ISO standard for gloss measurements [17].

The gloss level of each sample was determined for the 60-degree measurement angle and compared to the m parameter extracted from the fitted Cook-Torrance BRDF models. Here, a larger value for m corresponds to rougher surfaces with a wider, more diffuse specular lobe and therefore less specular reflection.

Figure 8 shows the comparison described in the previous paragraph. Note that although these data are based on measurements obtained with different instruments, they show a fairly good correlation. Furthermore, we can see the expected trend where smoother surfaces (low roughness values) correspond to higher gloss levels. Finally, we see that patches of different colors exhibit a similar relationship between the roughness and gloss levels. This indicates that the gloss meter measurements are not strongly affected by the surface color.

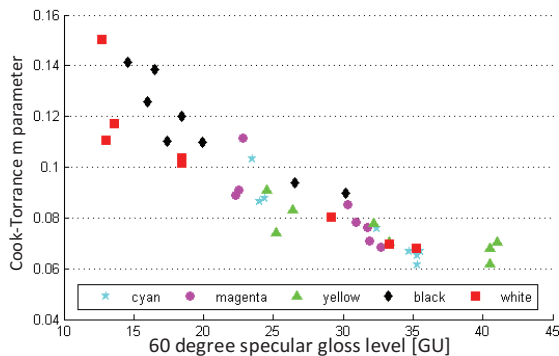


Figure 8. Comparing m parameter of flat gloss samples from Cook-Torrance model fitting with specular gloss level as measured using a gloss meter instrument.

Conclusion

In this paper, we mainly discussed BRDF measurements and model fitting for relief printing. The fitting results show that the Ward model can characterize the ink and printing process that we use better than the other models we tested. We also demonstrated correlation between Cook-Torrance m parameter and surface roughness and gloss level, respectively. This study is a useful starting point to further study how to produce desired BRDFs using a relief printer.

References

- [1] X. Liu, L. Chen, M. V. Ortiz Segovia, J. Ferwerda, and J. P. Allbach, "Characterization of relief printing", in *IS&T/SPIE Electronic Imaging: Measuring, Modeling, and Reproducing Material Appearance*, San Francisco, 2014.
- [2] T. Weyrich, et al. "Fabricating microgeometry for custom surface reflectance." *ACM Transactions on Graphics (TOG)*. Vol. 28. No. 3. ACM, 2009.
- [3] Y. Lan, et al. "Bi-scale appearance fabrication." *ACM Transactions on Graphics (TOG)* Vol. 32.4, pg. 145, 2013.

- [4] M. Ashikhmin, and S. Premoze. "Distribution-based brdfs." Unpublished Technical Report, University of Utah 2, 2007.
- [5] J. F. Blinn, "Models of light reflection for computer synthesized pictures." *ACM SIGGRAPH Computer Graphics*. vol. 11.2, pg. 192-198. (1977).
- [6] G. J. Ward, "Measuring and modeling anisotropic reflection." *ACM SIGGRAPH Computer Graphics* vol. 26.2, pg. 265-272. (1992).
- [7] R. L. Cook, and K. E. Torrance. "A reflectance model for computer graphics." *ACM Transactions on Graphics (TOG)* vol. 1.1, pg. 7-24. (1982).
- [8] M. Ashikhmin, S. Premoze, and P. Shirley. "A microfacet-based BRDF generator." *Proc. of the 27th annual conference on Computer graphics and interactive techniques*. ACM, pg. 65-74. (2000).
- [9] A. Ngan, F. Durand, and W. Matusik. "Experimental validation of analytical BRDF models." *ACM SIGGRAPH 2004 Sketches*. ACM, 2004.
- [10] P. Shirley, "Monte carlo methods in rendering." *ACM SIGGRAPH 96 Course Notes CD-ROM-Global Illumination in Architecture and Entertainment*, pg. 1-26, 1998.
- [11] T. Baar, H. Brettel, and M. V. Ortiz Segovia, "Towards gloss control in fine art reproduction." in *IS&T/SPIE Electronic Imaging: Measuring, Modeling, and Reproducing Material Appearance*, San Francisco, 2015.
- [12] R. Montes Soldado, and U. Carlos, "An Overview of BRDF Models." 2012.
- [13] R. Cook, K. Torrance, "A reflection model for computer graphics", *ACM Transactions On Graphics* 1, no. 1, pg. 7-24, 1982.
- [14] D. Kroese, and Z. Botev. "Spatial process generation." *arXiv preprint arXiv:1308.0399*, 2013.
- [15] K. Torrance, E. Sparrow, "Theory for off-specular reflection from rough surfaces", *Journal of Optical Society of America*, vol. 57, pg. 1105-1114, 1967.9.
- [16] R. J. Wagner, "Shadowing of randomly rough surfaces." *The Journal of the Acoustical Society of America* Vol. 41, pg. 138-147, 1967.1.
- [17] ISO 2813-2014 S. Paints and varnishes — Determination of gloss value at 20 degrees, 60 degrees and 85 degrees ISO (ISO, Geneva), www.iso.org.

Author Biography

Ni Yan received her BE in Electrical Engineering from Beijing University of Posts and Telecommunications, Beijing, China (2012) and she is currently a PhD student in Purdue University, West Lafayette, IN, U.S.A. She has mainly focused on image quality assessment as a research assistant in Purdue. And she had a 7-month internship with Océ – Canon Group, France, where she did the study in this paper.

Teun Baar recently finished a PhD at Mines-Telecom, Paris in collaboration with Océ-CANON, after receiving his Master's degree in Applied Physics from the Delft University of Technology. In his research, Teun focused on the optimization of print quality with multi-channel

printing systems, in particular 3D printing and the perception and control of print surface characteristics such as color, gloss, and BRDF. His research interests include reproduction and perception of material

appearance, 3D printing, color science, and surface perception, among others.